Kirchhoff-Love shell formulation based on triangular isogeometric analysis

Mehrdad Zareh, Xiaoping Qian
University of Wisconsin-Madison

January 19, 2019

Highlights:

- Rational triangular Bézier splines (rTBS) is used for developing finite shell elements based on Kirchhoff-Love shells. Using the proposed technique we can achieve three major goals:
- Analysis of Geometric models of complex topology;
- Efficient local mesh refinement;
- Optimal convergence rate.

Abstract- This article presents application of rational triangular Bézier splines (rTBS) for developing Kirchhoff-Love shell elements in the context of isogeometric analysis. Kirchhoff-Love shell formulation requires high continuity between elements because of higher order PDEs in the description of the problem; therefore, the non-uniform rational B-spline (NURBS)-based IGA has been extensively used for developing Kirchhoff-Love shell elements, as NURBS-based IGA can provide high continuity between and within elements; however, NURBS-based IGA has some limitations; such as, analysis of a complex geometry might need multiple NURBS patches and imposing higher continuity constraints over interfaces of patches is a challenging issue. Addressing these limitations, isogeometric analysis based on rTBS can provide C1 continuity over the mesh including element interfaces, a necessary condition in finite elements formulation of Kirchhoff-Love shell theory. Based on this technology, we use Cr smooth rational triangular Bézier spline as the basis functions for representing both geometry and solution field. In addition to providing higher continuity for Kirchhoff-Love formulation, using rTBS elements we can achieve three significant challenging goals: optimal convergence rate, efficient local mesh refinement and analysis of geometric models of complex topology. The proposed method is applied on several examples; first, this technique is verified against multiple plate and shell benchmark problems; investigating the convergence rate on the benchmark problems demonstrate that the optimal convergence rate can be obtained by the proposed technique. We also apply our method on geometric models of complex topology or geometric models in which efficient local refinement is required. Moreover, a car hood is modeled with rTBS and structurally analyzed by using the proposed framework.

keywords: Isogeometric Analysis, Shell elements, Kirchhoff-Love Shell, Rational Triangular Bézier Splines (rTBS), Complex Geometry.

1 INTRODUCTION

Mechanical analysis of thinned-wall structures, shells, has always been an appealing topic in engineering, owing to its key role in structural design and the complexity in the physics of the problem. From computational standpoint, mathematics of shell and plate formulations has drawn great attention; hence, there are manifold theories of shells and plates with respect to the numerical application. Among these theories, Kirchhoff-Love and Reissner-Mindlin theories have been extensively employed for developing finite element formulation of shells and plates mechanics. The major difference between these two theories arises from physical description of problem; in Kirchhoff-Love, the normal to the midsurface is assumed to remain normal after deformation. However, in Reissner-Mindlin, this normal can rotate after deformation [1]. The Reissner-Mindlin formulation is relatively more accurate for thick shells and it is generally used for this type of shells [2].

Although thin shell definition encompasses most shell structures in engineering practice, Reissner-Mindlin is more attractive for application in finite element software because the C0-continuity over elements interfaces is sufficient in Reissner-Mindlin based FEM, while Kirchhoff-Love models require C1-continuity over elements and their interfaces[3]. Despite many efforts for imposing C1-continuity on Lagrange elements (e.g. [4, 5, 6, 7] and references therein), the developed formulations are generally complex and expensive to implement. Hence, finite shell and plate elements derived from Reissner-Mindlin theory are more widely used[8, 9, 10]. There are also some other techniques in this regard, such as rotation-free thin shells with subdivision finite elements[11, 12], extended rotation-free shells including transverse shear effects [13], meshfree Kirchhoff-Love shells[13] and discontinuous Galerkin method for Kirchhoff-Love shells [14, 15]. Recently, Greco et. al [16] proposed a bi-cubic G1-

conforming element for Kirchhoff plate model; using Lagrange multiplier and penalty formulation they have achieved optimal convergence rate.

The Kirchhoff-Love model is appealing for numerical analysis due to its relatively fewer degrees of freedom; using this theory, only the displacement fields have to be computed,[17, 18, 19], whereas Reissner-Mindlin formulation requires both displacements and rotation fields. Furthermore, Kirchhoff-Love formulation does not suffer from the shear locking existing in Reissner-Mindlin shell and plate elements[19].

Isogeometric analysis (IGA), a new framework for finite element analysis introduced by Hughes et al. [20], has become an appealing technology for the numerical modeling due to its attractive properties, e.g. exact geometry representation, higher convergence rate and achievable continuity within and between elements. These features, in particular the continuity, have made IGA a promising framework for shell and plate elements [21]. Initially, IGA was based on representing both geometry and the unknown (solution) fields by non-uniform B-splines (NURBS) of high regularity. Smooth NURBS functions can conveniently provide higher continuities. Kiendl et al. [22] introduced the application of IGA for developing Kirchhoff-Love shell elements. This work was followed by many other studies;[23, 24, 25, 26, 27, 28, 28] on various Reissner-Mindlin shells with isogeometric analysis. The hierarchic family of isogeometric shell elements introduced by Echter et al. [29] includes 3-parameter (Kirchhoff-Love), 5-parameter (Reissner-Mindlin) and 7-parameter (three-dimensional shell) models. Solid-shell elements based on isogeometric NURBS were investigated by Bouclier et al. [30], Hosseini et al. [31, 32], Du et al. [21]. The shell formulation of Benson et al. [33] blended and used both Kirchhoff-Love and Reissner-Mindlin theories.

Despite showing significant advantages, NURBS-based IGA has some limitations such as lack of automatic parametrization, inefficient local mesh refinement and difficulties in complex topology representation [34, 35, 36, 37]. The problem of local mesh refinement has been addressed by polynomial splines over hierarchical T-meshes (PHT-splines) [38]. In the literature, the latter two issues have been dealt with mostly by dividing the physical domain into multiple patches; this method gives rise to challenging complexities regarding the continuity over the interfaces of patches [21]. Mortar, penalty method and Nitsche method, despite their limitations, have been used to resolve the issue; Du et al. [21] employed the Nitsche method for isogeometric analysis of a plate comprised of non-conforming multi-patches. Also, the same method has been used by [39] for enforcing coupling constraints at trimming curves of thin shells. In a study by Kiendl et al. [40], they used the bending strip method to impose the C1-continuity over shell structures represented with multiple patches.

Considering limitations of NURBS-based IGA, we seek other techniques. Rational triangular Bézier splines (rTBS), an alternative to NURBS, was developed in the context of analysis by Qian's group [41]. The rTBS framework has been improved by Xia et. al.[34, 42]; they achieved high continuity between patches and applied the improved framework on various partial differential equations including elasticity problem over 2D and 3D domains. Recently, rTBS has been used for developing Kirchhoff-Love plate elements in [43]; they could obtain continuity over mesh by using Lagrange multipliers. Moreover, their work is limited to only plate formulation. Addressing the aforementioned challenges and limitations, this study aims at developing a novel Kirchhoff-Love shell and plate elements formulation based on the improved (rTBS) which provides the essential C1 continuity of Kirchhoff-Love formation. We use Cr smooth rational triangular Bézier spline as the basis functions for representation of both geometry and solution field. Geometry is discretized into a set of Cr rTBS elements while the input geometry boundary is preserved. It is worthwhile clarifying the definition of Cr smoothness in the article; this implies that two polynomial functions in adjacent elements join r times differentiably across the boundary. The Cr smoothness of the basis allows us to develop Kirchhoff-Love plate and shell elements. In addition to the important contribution regarding continuity for Kirchhoff-Love shell formulation, three significant objectives are achieved: optimal convergence rate, efficient local mesh refinement and analysis of geometric models of complex topology. These contributions are demonstrated through several examples. First, we investigate the accuracy and convergence rate of the current method by applying it on multiple benchmarks problems, for both plate and shell elements. In the last example, the proposed method is used to model and analyze a car hood; this example demonstrates the applicability of the current technology on real engineering problems.

2 Formulations and Methods

This section presents the mechanics of thin shells, discretization and rational triangular Bézier splines. A brief introduction on the mechanics of thin shells will allow us to clearly explain how we use rTBS for solving the equations of thin shell mechanics.

2.1 Mechanics of thin shell

The formulation of thin shells mechanics are described, i.e., kinematics of thin shells (based on Kirchhoff-love theory) and constitutive relations are briefly explained.

In the theory of Kirchhoff-Love shells, shell structure is assumed to be thin such that transverse shear strains can be assumed negligible. This assumption implies that a vector normal to the mid-surface remains normal after deformation and the shell geometry description is reduced to its mid-surface[44]. The following formulations are based on [38]. The Greek index $\alpha = 1, 2$ denotes quantities in curvilinear coordinate

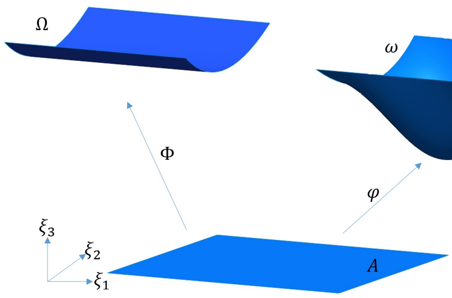

Figure 1: Shell geometry. A denotes the parametric domain, Φ and ϕ represents the shell geometry before and after deformation, respectively.

system. Also, capital letters are used for configuration before deformation. The shell middle surface is parametrized by coordinates $\xi^1, \xi^2 \in A \subset \Re^2$ (see Fig. 1). The position of a material point in the reference configuration is defined by

$$X(\xi^1, \xi^2, \xi^3) = \Phi(\xi^1, \xi^2) + \xi^3 T(\xi^1, \xi^2), \tag{1}$$

and deformed configuration

$$x(\xi^1, \xi^2, \xi^3) = \phi(\xi^1, \xi^2) + \xi^3 t(\xi^1, \xi^2), \tag{2}$$

where t is the normal to surface and $\zeta \in [-0.5h, 0.5h]$ is the coordinate within the thickness and h denotes the thickness. The functions $\Phi(\xi^1, \xi^2)$ and $\phi(\xi^1, \xi^2)$ map middle surface from the parametric domain to the physical space, for reference and deformed configuration. Kirchhoff-Love hypothesis implies that T and t are perpendicular to Φ_α and ϕ_α

$$T = \frac{\Phi_{,1} \times \Phi_{,2}}{||\Phi_{,1} \times \Phi_{,2}||}, \quad t = \frac{\phi_{,1} \times \phi_{,2}}{||\phi_{,1} \times \phi_{,2}||}, \tag{3}$$

$$\Phi_{,\alpha} \cdot T = 0, \quad |T| = 1, \quad T \cdot T_{,\alpha} = 0. \tag{4}$$

The deformation gradient is defined by

$$F = \nabla x \cdot (\nabla X)^{-1}, \quad \nabla x = \begin{bmatrix} \frac{\partial x_1}{\partial \xi_1} & \frac{\partial x_1}{\partial \xi_2} & \frac{\partial x_1}{\partial \xi_3} \\ \frac{\partial x_2}{\partial \xi_1} & \frac{\partial x_2}{\partial \xi_2} & \frac{\partial x_2}{\partial \xi_3} \\ \frac{\partial x_3}{\partial \xi_1} & \frac{\partial x_3}{\partial \xi_2} & \frac{\partial x_3}{\partial \xi_3} \end{bmatrix}. \tag{5}$$

The covariant base vectors are given by

$$
\begin{aligned}
g_\alpha = \frac{\partial x}{\partial \xi^\alpha} = \phi_{,\alpha} + \xi^3 t_\alpha, \quad g_3 = \frac{\partial x}{\partial \xi^3} = t, \\
G_\alpha = \frac{\partial X}{\partial \xi^\alpha} = \Phi_{,\alpha} + \xi^3 T_\alpha, \quad G_3 = \frac{\partial X}{\partial \xi^3} = T.
\end{aligned} \tag{6}
$$

The Green-Lagrange strain tensor is defined by

$$
E = \frac{1}{2}(F^T F - I), \tag{7}
$$

where F and I denotes the deformation gradient and identity tensor, respectively.

The strain tensor components are decomposed into membrane and bending contributions.

$$
\begin{aligned}
E_{\alpha\beta} = \epsilon_{\alpha\beta} + \xi^3 \kappa_{\alpha\beta} = \frac{1}{2}(g_{\alpha\beta} - G_{\alpha\beta}) + \xi^3(k_{\alpha\beta} - K_{\alpha\beta}), \\
g_{\alpha\beta} = g_{,\alpha} \cdot g_{,\beta} = x_{,\alpha} \cdot x_{,\beta}, \\
G_{\alpha\beta} = G_{,\alpha} \cdot G_{,\beta} = X_{,\alpha} \cdot X_{,\beta}, \\
k_{\alpha\beta} = -g_{\alpha\beta} \cdot t, \quad K_{\alpha\beta} = -G_{\alpha\beta} \cdot T.
\end{aligned} \tag{8}
$$

Using constitutive relations, we can define stress tensor (Voigt notation)

$$
\sigma = \begin{bmatrix} \sigma^{11} \\ \sigma^{22} \\ \sigma^{12} \end{bmatrix} = \frac{E}{1-\nu^2} \begin{bmatrix} 1 & \nu & 0 \\ \nu & 1 & 0 \\ 0 & 0 & \frac{1-\nu}{2} \end{bmatrix} \begin{bmatrix} E_{11} \\ E_{22} \\ 2E_{12} \end{bmatrix}, \tag{9}
$$

where E is the Youngs modulus and ν denotes the Poissons ratio. The stresses are decomposed into a membrane and a bending stress; after integrating through the thickness,force and moment resultants are defined

$$
n = \begin{bmatrix} n^{11} \\ n^{22} \\ n^{12} \end{bmatrix} = \frac{Eh}{1-\nu^2} \begin{bmatrix} 1 & \nu & 0 \\ \nu & 1 & 0 \\ 0 & 0 & \frac{1-\nu}{2} \end{bmatrix} \begin{bmatrix} \epsilon_{11} \\ \epsilon_{22} \\ 2\epsilon_{12} \end{bmatrix}, \tag{10}
$$

$$
m = \begin{bmatrix} m^{11} \\ m^{22} \\ m^{12} \end{bmatrix} = \frac{Eh^3}{12(1-\nu^2)} \begin{bmatrix} 1 & \nu & 0 \\ \nu & 1 & 0 \\ 0 & 0 & \frac{1-\nu}{2} \end{bmatrix} \begin{bmatrix} \kappa_{11} \\ \kappa_{22} \\ 2\kappa_{12} \end{bmatrix}. \tag{11}
$$

To obtain the equilibrium between internal forces ans external loads, we can use the principle of virtual work expressed as

$$
\delta w = \delta w_{int} + \delta w_{ext} = 0, \tag{12}
$$

in which internal and external virtual work is given by

$$\delta w_{int} = -\int_{\Omega} (\sigma \cdot \delta E) d\Omega = -\int_{\mathbf{A}} (n \cdot \delta\epsilon + m \cdot \delta\kappa) j d\xi^1 \xi^2, \tag{13}$$

$$\delta w_{ext} = \int_{\Omega} (q \cdot \delta u) d\Omega + \int_{\Gamma_t} (p \cdot \delta u) d\Gamma, \tag{14}$$

where $j = ||\Phi_{,1} \times \Phi_{,2}||$. we note that δE, δu, q and p and refer to variation of the strain, variation of the displacement, body force and traction force, respectively.

2.2 Isogeometric Discretization

Based on the concept of isogeometric analysis, both shell surface and solution field (displacement) are defined in terms of same basis functions

$$\Phi(\xi^1, \xi^2) = \sum_{i=1}^{n} N(\xi^1, \xi^2) P^i, \tag{15}$$

$N(\xi^1, \xi^2)$ and P^i are the basis functions and control points, respectively. These terms will be detailed in the next section.

$$u(\xi^1, \xi^2) = \sum_{i=1}^{n} N(\xi^1, \xi^2) u^i. \tag{16}$$

The membrane and bending strain can then be discretized by

$$\epsilon(\xi^1, \xi^2) = \sum_{i=1}^{n} B_n^i(\xi^1, \xi^2) u^i, \tag{17}$$

$$\kappa(\xi^1, \xi^2) = \sum_{i=1}^{n} B_m^i(\xi^1, \xi^2) u^i, \tag{18}$$

where

$$B_n^i = \begin{bmatrix} N_{,1}^i \Phi_{,1} \cdot e_1 & N_{,1}^i \Phi_{,1} \cdot e_2 & N_{,1}^i \Phi_{,1} \cdot e_3 \\ N_{,2}^i \Phi_{,2} \cdot e_1 & N_{,2}^i \Phi_{,2} \cdot e_1 & N_{,2}^i \Phi_{,2} \cdot e_3 \\ (N_{,2}^i \Phi_{,1} + N_{,1}^i \Phi_{,2}) \cdot e_1 & (N_{,2}^i \Phi_{,1} + N_{,1}^i \Phi_{,2}) \cdot e_2 & (N_{,2}^i \Phi_{,1} + N_{,1}^i \Phi_{,2}) \cdot e_3 \end{bmatrix},$$

$$B_m^i = \begin{bmatrix} B_{m11}^i \cdot e_1 & B_{m11}^i \cdot e_2 & B_{m11}^i \cdot e_3 \\ B_{m22}^i \cdot e_1 & B_{m22}^i \cdot e_2 & B_{m22}^i \cdot e_3 \\ 2B_{m12}^i \cdot e_1 & 2B_{m12}^i \cdot e_2 & 2B_{m12}^i \cdot e_3 \end{bmatrix},$$

$$\begin{aligned} B_{m\alpha\beta}^i = {} & \Phi_{,\alpha\beta} \cdot T \frac{1}{j} [N_{,1}^i (\Phi_{,2} \times T) - N_{,2}^i (\Phi_{,1} \times T)] + \\ & + \frac{1}{j} [N_{,1}^i (\Phi_{,\alpha\beta} \times \Phi_{,2}) - N_{,2}^i (\Phi_{,\alpha\beta} \times \Phi_{,1})] - N_{,\alpha\beta}^i \cdot T, \end{aligned} \tag{19}$$

N^i refers to the i-th basis function and e_1, e_2, e_3 denote the basis vectors of an orthonormal coordinate system. Considering equations. (10-18), we can create a set of equations, $Ku = f$, to find the unknowns u. K, stiffness matrix, and f, external load, are define by (before element assembly)

$$K^{ij} = \int_{\mathbb{A}} (h(B_n^i)^T D B_n^j + \frac{h^3}{12} (B_m^i)^T D B_m^j) j d\xi^1 \xi^2, \tag{20}$$

$$f_i = \int_{\mathbb{A}} q N_i j d\xi^1 \xi^2 + \int_{\partial \mathbb{A}} p N_i ||\Phi_{,t}|| dl_\xi. \tag{21}$$

2.3 IGA Based on Rational Triangular Bézier Splines

This section presents IGA on triangulation based on [34]. Each knot span in a NURBS curve corresponds to a Bézier curve which is defined by Bernstein basis functions. Bernstein polynomial of degree d is given by

$$\psi_{\mathbf{i},d}(\xi) = \frac{d!}{i!j!} \zeta^i (1-\zeta)^j, \quad | \mathbf{i} |= i + j = d. \tag{22}$$

In this study we use Bézier triangles. Bézier triangles are based on bivariate Bernstein polynomials. Bivariate form of Eqn. 22 describes the bivariate Bernstein polynomials:

$$\psi_{\mathbf{i},d}(\boldsymbol{\zeta}) = \frac{d!}{i!j!k!} \zeta_1^i \zeta_2^j \zeta_3^k, \quad | \mathbf{i} |= i + j + k = d, \tag{23}$$

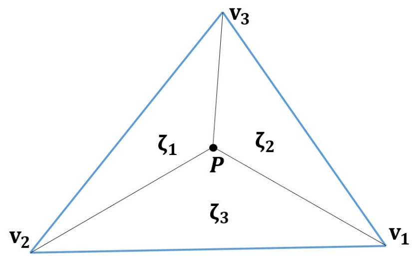

Figure 2: Barycentric coordinates of a point, $P(s,t)$, in a triangle, τ. $\zeta_1 = \frac{area(V_3V_2P)}{area(V_1V_2V_3)}$, $\zeta_2 = \frac{area(V_3V_1P)}{area(V_1V_2V_3)}$, $\zeta_3 = \frac{area(V_1V_2P)}{area(V_1V_2V_3)}$.

$\mathbf{i}$ refers to a triple index i, j, k. $\zeta_1, \zeta_2, \zeta_3$ are the barycentric coordinates of a point $(s,t) \in \mathbb{R}^2$. Any points in a fixed triangle τ defined by vertices $\mathbf{v}_1, \mathbf{v}_2, \mathbf{v}_3$ (see Fig. 2) can be described uniquely by

$$(s,t) = \zeta_1\mathbf{v}_1 + \zeta_2\mathbf{v}_2 + \zeta_3\mathbf{v}_3, \quad \zeta_1 + \zeta_2 + \zeta_3 = 1. \tag{24}$$

Given the above information, we can define a triangular Bézier patch

$$\mathbf{x}(\boldsymbol{\zeta}) = \sum_{|\mathbf{i}|=d} \mathbf{p_i}\psi_{\mathbf{i},d}(\boldsymbol{\zeta}), \tag{25}$$

$\mathbf{p_i}$ is a set of control points. By considering weights, A rational Bézier triangle is given by

$$\mathbf{x}(\boldsymbol{\zeta}) = \sum_{|\mathbf{i}|=d} \mathbf{p_i}\Psi_{\mathbf{i},d}(\boldsymbol{\zeta}), \tag{26}$$

where

$$\Psi_{\mathbf{i},d} = \frac{w_{\mathbf{i}}\psi_{\mathbf{i},d}}{\displaystyle\sum_{|\mathbf{i}|=d} w_{\mathbf{i}}\psi_{\mathbf{i},d}} \tag{27}$$

$w_{\mathbf{i}}$ refers to the weight of the control point $\mathbf{p_i}$. Isoparametric concept implies that we can use the same bivariate Bernstein basis on a triangle τ with vertices $\mathbf{v}_1, \mathbf{v}_2, \mathbf{v}_3$ for defining a d-degree polynomial function f over τ as

$$f(\boldsymbol{\zeta}) = \sum_{|\mathbf{i}|=d} b_{\mathbf{i}}\Psi_{\mathbf{i},d}(\boldsymbol{\zeta}), \tag{28}$$

The $b_{\mathbf{i}}$ (or b_{ijk}) refer to the Bézier ordinates of f; their corresponding array of domain points are given by

$$q_{ijk} = \frac{i\mathbf{v}_1 + j\mathbf{v}_2 + k\mathbf{v}_3}{d}, \; i+j+k = d. \tag{29}$$

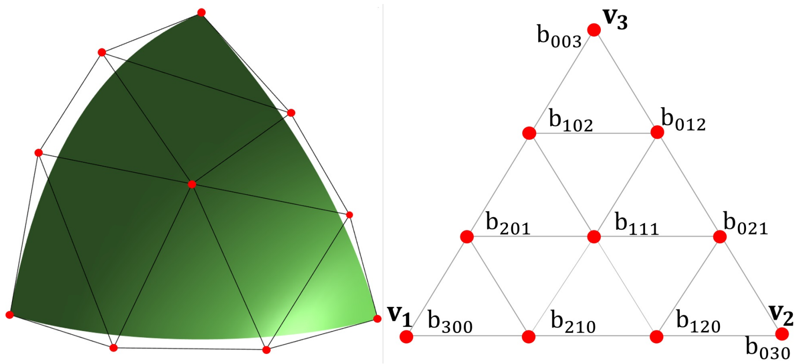

(a) Triangular Bézier patch. (b) Associated domain points of the Bézier ordinates b_{ijk} in $\{\mathbf{v_1}, \mathbf{v_2}, \mathbf{v_3}\}$.

Figure 3: Triangular Bézier patch and domain points.

The control polygon of the function f is determined by the points (q_{ijk}, b_{ijk}). Fig. 3 shows an example of a triangular Bézier patch and the associated domain points of the Bézier ordinates.

Continuity within and between elements is the key requirement in finite shell element based on Kirchhoff-love theory. C0 conforming triangular elements is one of the techniques to develop Kirchhoff-love shell elements, in which rotation is calculated as a degree of freedom. In the present method, however, rotation is not needed to be considered as a degree of freedom. Here, we describe how we obtain high continuity over triangular Bézier patches. Two degree-d polynomials f and $\tilde{f}$ join r times differentiably across the interface of two triangles $\tau = \{\mathbf{v}_1, \mathbf{v}_2, \mathbf{v}_3\}$ and $\tilde{\tau} = \{\mathbf{v}_4, \mathbf{v}_2, \mathbf{v}_3\}$ if and only if [45];$(j + k + \rho = d,\ \rho = 0, ..., r,)$

$$b^{\tilde{}}_{\rho,j,k} - \sum \frac{\rho!}{\mu!\nu!\kappa!} b_{\mu,k+\nu,j+\kappa} \zeta_1^{\mu}, \zeta_2^{\nu}, \zeta_3^{\kappa} = 0, \tag{30}$$

where $\zeta_1, \zeta_2, \zeta_3$ define the barycentric coordinates of vertex v4 in relation to triangle τ. Fig. 4 demonstrate two triangular Bézier patches with C1 continuity across the boundary of patches. The red solids represent free nodes of which values are independently computed; these nodes determine the value of black solids, dependent nodes, by applying the continuity constraints. The continuity constraints are imposed over the gray area; this figure also illustrates the coplanarity of the control points in these triangle pair.

Considering a parametric domain $\hat{\Omega}$ and its triangulation $\hat{T}$ (Fig. 5), the spline

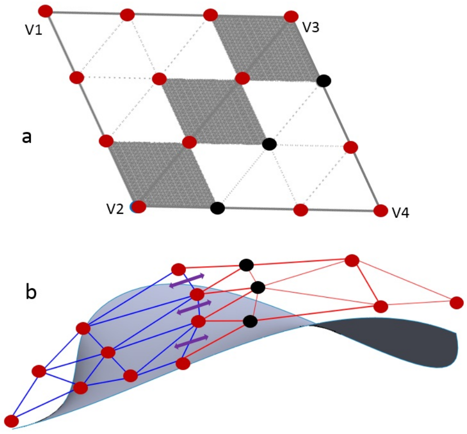

Figure 4: Illustration of dependent and independent nodes. a) Two domain triangles, b) two Bézier patches with c1 continuity. the red nodes represent free nodes whose values can be independently set, these nodes determine the value of black nodes, dependent nodes, through the continuity constraints. The shaded area shows the triangles where continuity constraints are imposed; figure b demonstrates that the control points in these triangle pair (indicated by $\longleftrightarrow$) are coplanar. For better visualization, the control net is shifted up slightly.

spaces of piecewise d-degree polynomials $\hat{T}$ is defined by [45]

$$\mathbf{S}_d^r(\hat{T}) = \left\{ f \in \mathbf{C}^r(\hat{\Omega}) : f|_\tau \in \mathbf{P} \ \forall \tau \in \hat{T} \right\}, \tag{31}$$

τ is an arbitrary triangle in $\hat{T}$ and r refers to the continuity order of the spline over $\hat{\Omega}$. A spline is called superspline when it has higher smoothness across some edges or at some vertices, and the associated space is given by [45]

$$\mathbf{S}_d^{r,\rho}(\hat{T}) = \left\{ f \in \mathbf{S}_d^r(\hat{T}) : f \in \mathbf{C}^{rv}(V) \ \forall v \in V \ \& \ f \in \mathbf{C}^{re}(e) \ \forall e \in E \right\}. \tag{32}$$

All vertices and edges are represented by V and E in $\hat{T}$ and $\rho := \{v\}_{v \in V} \cup \{e\}_{e \in E}$with $r \leq v, e \leq d$ for each $v \in V$ and $e \in E$. In order to obtain Cr spline spaces on a triangulated domain $\hat{\Omega}(\hat{T})$ multiple methods are available in the literature. Although, imposing condition (9) directly on the triangles is a conventional technique; the degree of the polynomial must be much higher than r, i.e. $d \geq 3r + 2$ [44]. In the present work, we also apply another method: splitting every triangle in $\hat{T}$ into multiple microtriangles before applying the continuity constraints on the microtriangles. Clough-Tocher (CT) and Powell-Sabin (PS) methods are used for splitting. In CT splitting method, each vertex of a triangle is connected to its centroid point; this

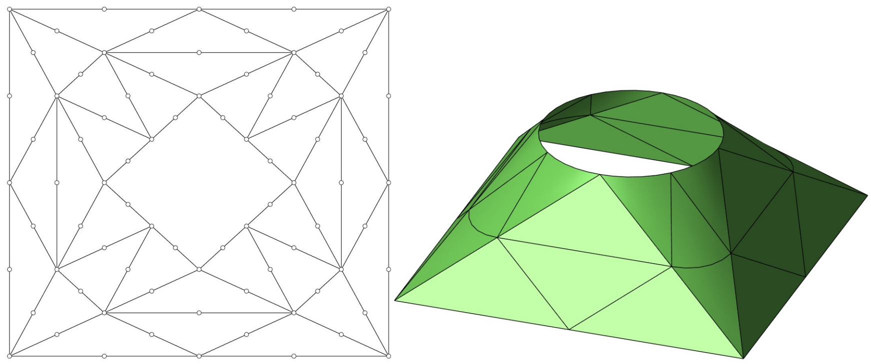

(a) Triangulated Parametric Domain (b) Triangulated Physical Domain

Figure 5: Illustration of a Triangulated physical and parametric Domain

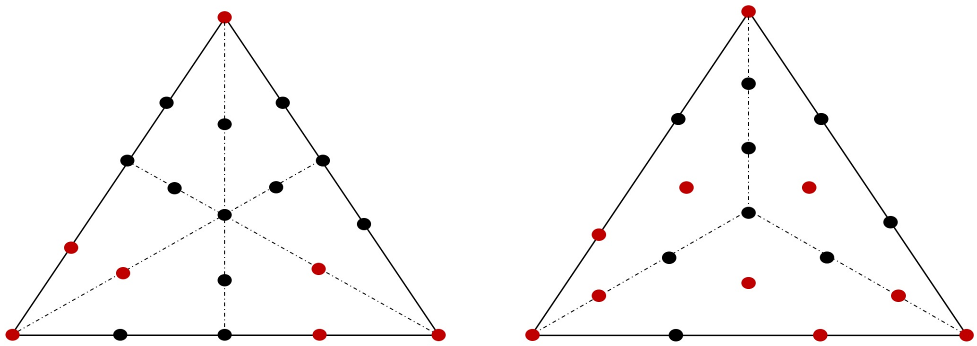

(a) PS macro-element (b) CT macro-element.

Figure 6: Splitting methods used in this study. red and black nodes represent independent and dependent nodes, respectively.

forms three micro-triangles. PS method splits each macro-triangle into six micro-triangles with centroid point as the interior split point. Edges are then bisected (see Fig. 6).

Using PS and CT macro-elements cannot guarantee obtaining optimal convergence rate. Possible inconsistency in geometric map during the refinement can damage the convergence rate; in order to avoid this inconsistency, we use smooth-refine-smooth procedure [42]. In this method, a sufficiently smooth pre-refinement map is constructed; then, further refinement can be applied and following C^r continuity constraints, rTBS elements are formed. The refined control points do not relocate as they have already satisfied the continuity conditions. The resulting mesh is C^r smooth, and the geometric map remains the same and doesn't suffer from inconsistency for all

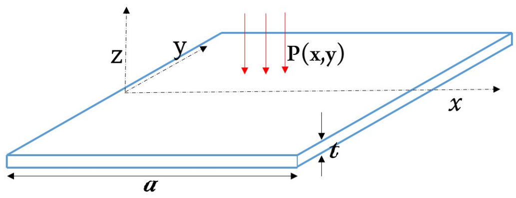

Figure 7: Problem setup. An isotropic square plate under a uniform transverse load; $\boldsymbol{t}$ and $\boldsymbol{a}$ refers to the thickness and side dimension of plate, respectively.

subsequent refinements. This remedy for inconsistency allows us to obtain optimal convergence rate. We also note that the initial geometry (surface) is C1 smooth.

In this study, the polynomial function is the displacement of the structure; following Galerkin method and FE discretization, the weighted basis function introduced in Eqn. (27) are plugged in B matrix, Eqn. (19). Also, the numerical integration is implemented in each element (if split is used, micro-element) by standard and collapsed [46] Gaussian quadrature rules on the boundaries and within element, respectively. Details on triangular Bézier patches and continuity constraints can be found in [34].

3 Numerical Results

3.1 Plates

This section presents numerical examples for K-L plate formulation. In the first two verification examples, convergence properties of the proposed approach are investigated. The third example, analyzing a geometric model of complex topology, demonstrates that the current method can be used for local mesh refinement and complex topology representation.

Convergence Study

In order to verify our method, an isotropic square plate under a uniform transverse load is analyzed (Fig. 7). The exact solution (Eqn. 33) is extracted from [47] for a square plate with simply supported boundary conditions. The simply supported boundary condition is applied as a Dirichlet B.C.; i.e. the displacement of boundary nodes are set to zero. We note that in plate formulation, the deformation distribution is calculated in one direction, i.e. degree of freedom per node is one.

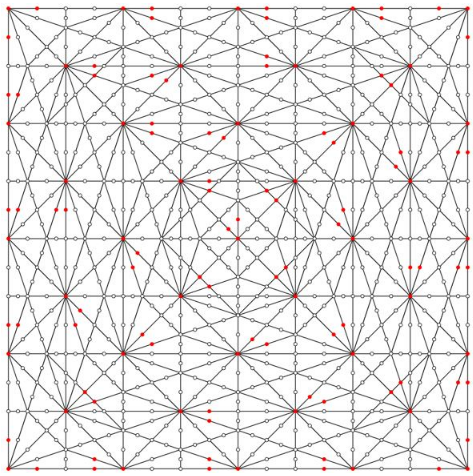

Figure 8: C1 continuous mesh with PS split for a square plate. The red solid nodes are free (independent) nodes whereas white solid nodes are dependent nodes; values of white nodes are determined through the continuity.

$$w = \frac{4qa^4}{\pi^5 D} \sum_{m=1,3,5,\ldots}^{\infty} \frac{1}{m^5}(1 - \frac{\alpha_m \tanh \alpha_m + 2}{2\cosh \alpha_m} \cosh \frac{2\alpha_m y}{a} + \\ + \frac{\alpha_m}{2\cosh \alpha_m} \frac{2y}{a} \sinh \frac{2\alpha_m y}{a}) \sin \frac{m\pi x}{a}, \tag{33}$$

where q, a and D represent transverse load, square dimension (see Fig. 7) and bending stiffness, respectively. Also the dimensionless $\alpha_m = \frac{m\pi}{2}$.
Fig. 8 illustrates the C1 continuous mesh for this problem. The red solid nodes are free (independent) nodes and white solid nodes are dependent nodes; the values of dependent nodes are determined through the continuity constraints, as explained in previous section.

Fig. 10 shows the results of the simulation when we set $a = 1, t = a/1000, q = 0.01$, $E = 10^7$ and $\nu = 0.3$. Fig. 11 illustrates the convergence rate for the simply supported plate under uniform load. Using quadratic polynomial ($p = 2$), cubic polynomial ($p = 3$) and quintic polynomials convergence rates (in L^2 norm) are found to be 2, 3.1 and 3.5, respectively. This is the best convergence rate for this problem; quadratic convergence rate for quadratic polynomial is consistent with error estimates proved in [48, 49, 44]; for PDEs of order $2m$ with $m \geq 1$ and exact solution $u \in H^r_\Omega$, r is the regularity, the error estimates in L^2 is given by

$$\|u - u_h\|_{L^2(\Omega)} \leq Ch^\beta \|u\|_{H^r_\Omega}, \tag{34}$$

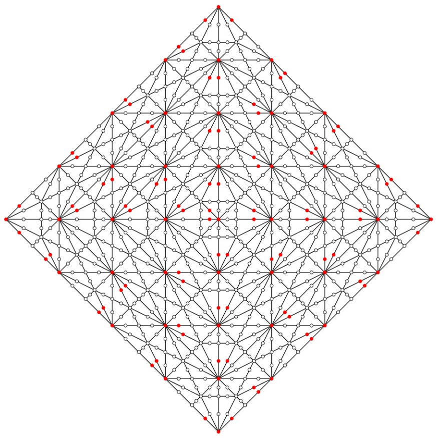

(a) Parametric Domain

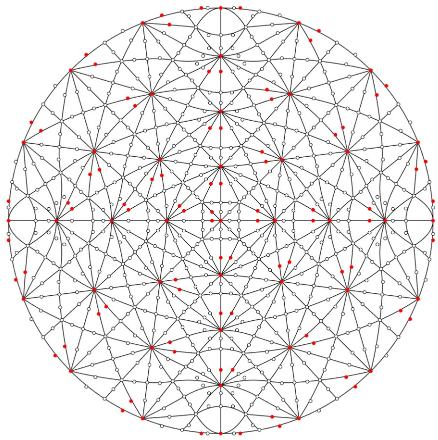

(b) Physical Domain

Figure 9: C1 continuous mesh with PS split for a circular plate.

h, C and β refer to the size of elements, a constant (independent of u and h) and a lower bound for the convergence order estimate, respectively. For Galerkin method β is defined by

$$\begin{aligned} \beta &= min\{\delta, 2(\delta - m)\}, \\ \delta &= min\{r, p+1\}, \end{aligned} \tag{35}$$

where p is the polynomial degree. For cubic and quintic the well-established optimal convergence rate of $p+1$ is not attainable, owing to the critical regularity of the exact solution ($r \leq p+1$) [44];for further details on regularity and optimal convergence rate, readers are referred to aforementioned reference.

In the second example, the proposed method is tested against the problem of simply supported circular plate under uniform loading. The exact solution (Eqn. (36) is extracted form [44]

$$u(r) = \frac{qr^4}{64D}(\frac{r^4}{R^4} - 2\frac{3+\nu}{1+\nu}\frac{r^2}{R^2} + \frac{5+\nu}{1+\nu}), \tag{36}$$

where r denotes the distance from the center of circle and R is the radius of circle.

Fig. 9 shows the C1 continuous mesh for circular plate. The red solid nodes are free (independent) nodes and white solid nodes are dependent nodes; the values of dependent nodes are determined through the continuity constraints, as explained in previous section.

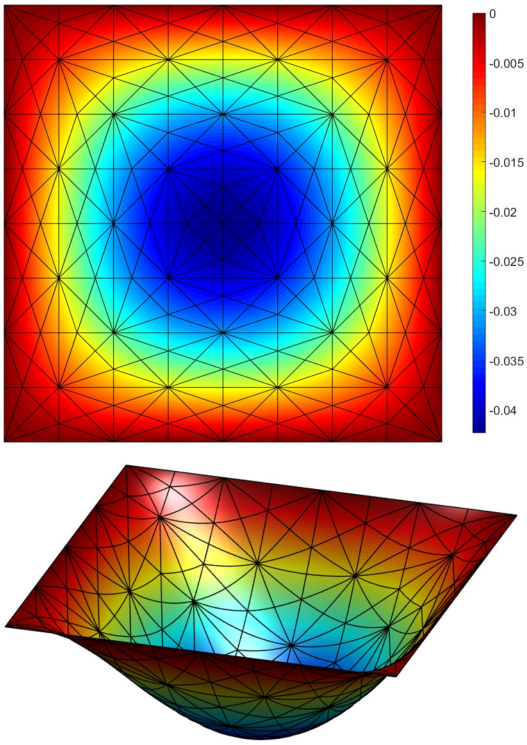

Figure 10: Computed deformation distribution of the isotropic square plate under a uniform transverse load. For a finer visualization in 3D view, numerical results are artificially scaled up.

Fig. 12 demonstrates the estimated deformation distribution for this problem. Fig. 13 illustrates the convergence rate for quadratic, cubic and quintic polynomials; optimal convergence rate is attained for all polynomials; for quadratic polynomials convergence rate is found to be approximately $p = 2$; differently from square plate analysis, optimal convergence rate $(p+1)$ is obtained for cubic and quintic polynomials because the exact solution does not hold any critical regularities.

Complex Topology and Local Refinement

The last example indicates the functionality of current technique for representing a geometric model of complex topology. Fig. 14 shows the mesh model (quadratic elements with PS split, number of free nodes=582) of a plate with three holes; the mesh is efficiently refined around the holes without refinement in the rest of the geometry. Local mesh refinement can be useful for error-adaptive mesh refinement. Fig. 15 demonstrates the computed deformation distribution in this plate; the model is under uniform distributed load and boundary edges are fixed.

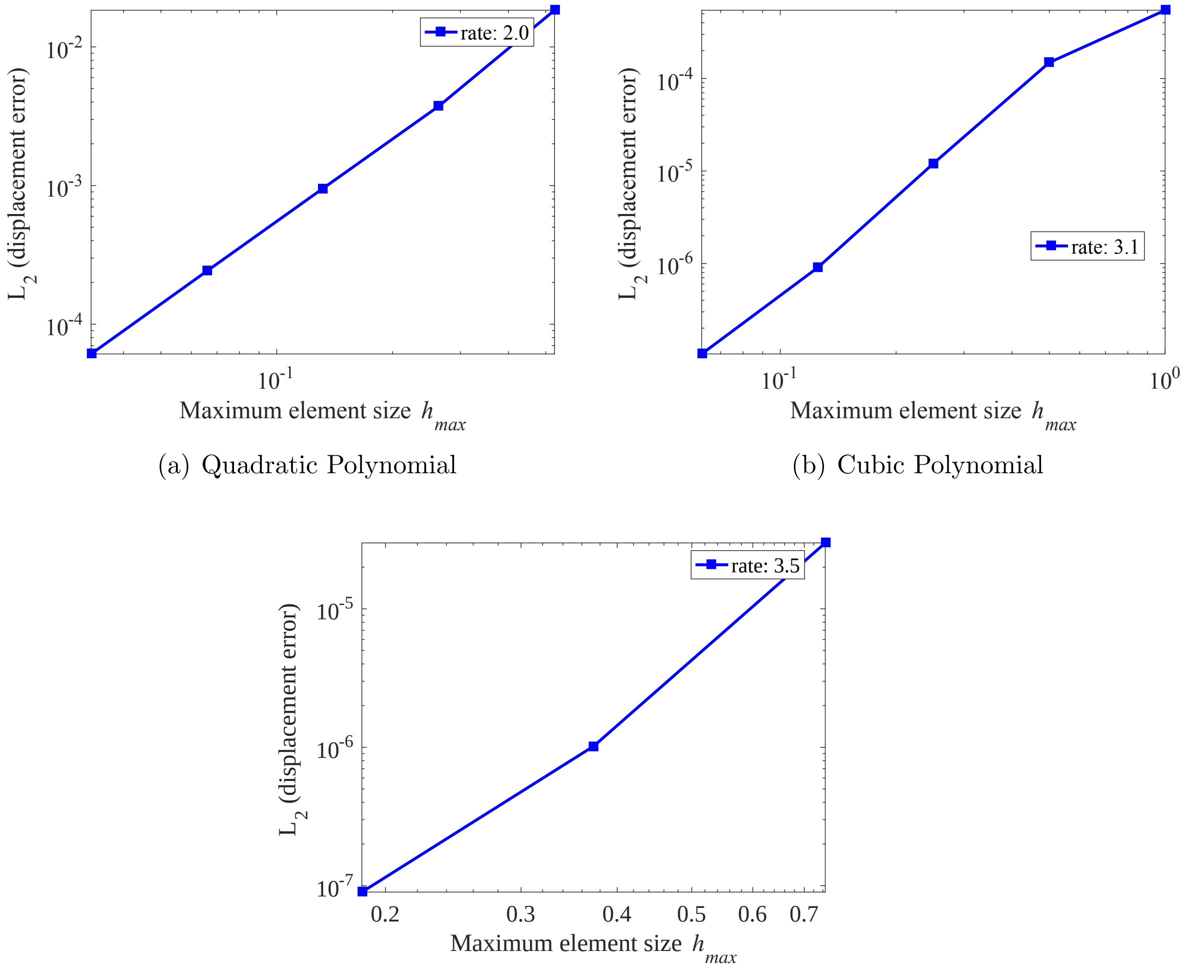

(a) Quadratic Polynomial

(b) Cubic Polynomial

(c) Quintic Polynomial

Figure 11: The convergence rate for the problem of simply supported plate under uniform load. For quadratic polynomial (a), cubic polynomial (b) and quintic polynomial (c) convergence rates are found to be 2, 3.1 and 3.5, respectively.

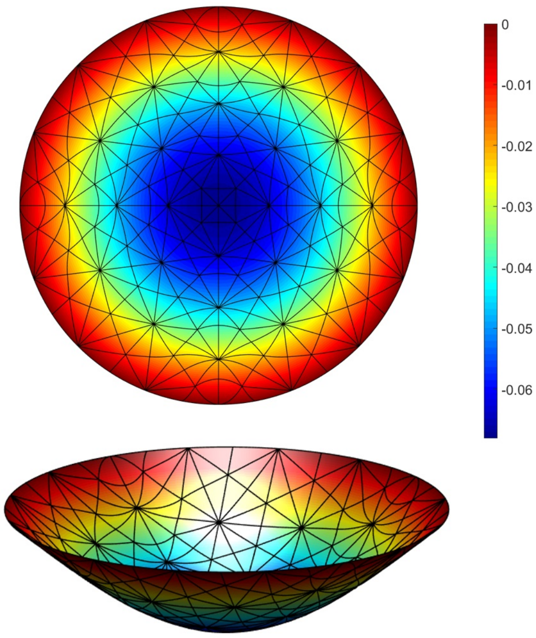

Figure 12: Computed deformation distribution of an isotropic circular plate under a uniform transverse load. For a better visualization in 3D view, numerical results are artificially scaled up.

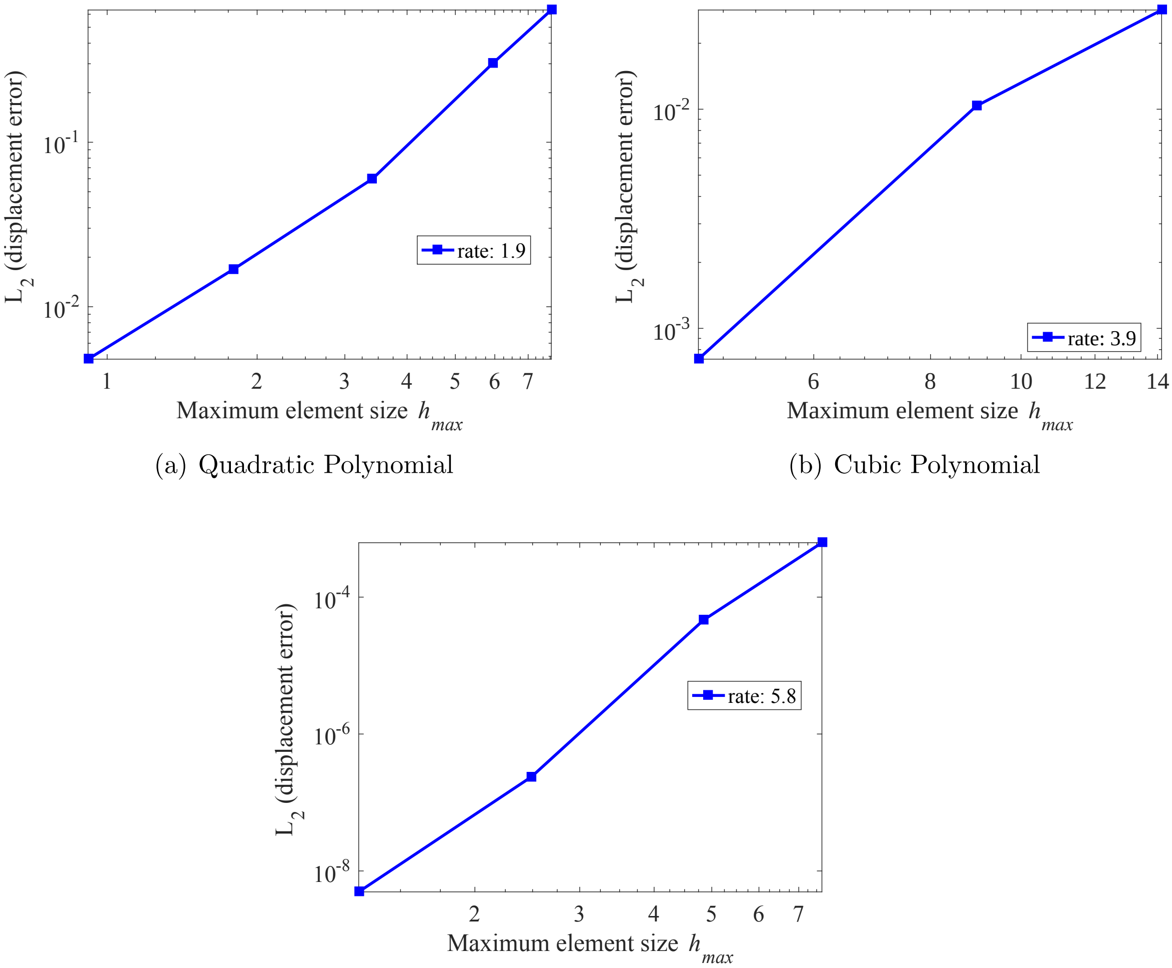

(a) Quadratic Polynomial

(b) Cubic Polynomial

(c) Quintic Polynomial

Figure 13: The convergence rate of circular plate analysis for quadratic (a), cubic (b) and quintic (c) polynomials; optimal convergence rate is attained for all cases.

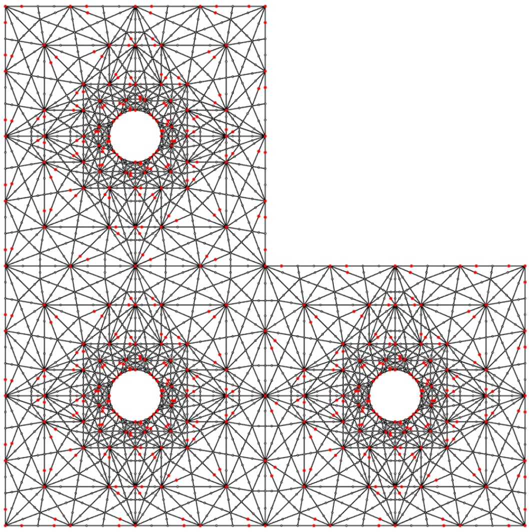

Figure 14: Mesh model (PS split) of a plate with three holes; mesh around the holes is locally refined without refinement in the rest of the geometry.

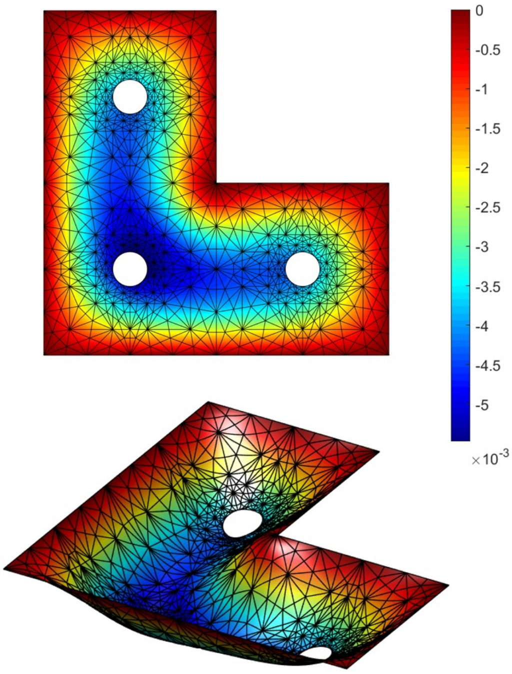

Figure 15: The deformation distribution in a plate with three holes; The plate is under uniform load and simply supported boundary conditions. For a better visualization in 3d view, numerical results are artificially scaled up.

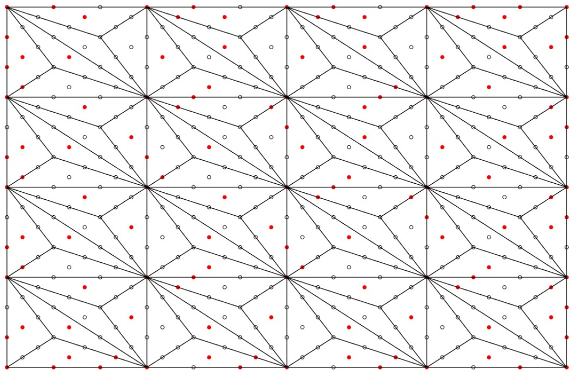

(a) Parametric Domain

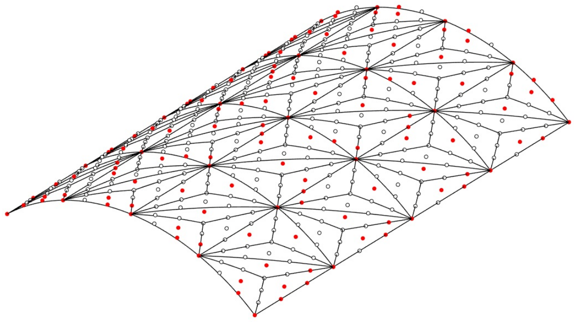

(b) Physical Space

Figure 16: Parametric and physical C1 mesh with CT split. We use cubic triangular elements.

3.2 Shell Structures

This section begins with a benchmark problem for verifying the proposed method for shell elements (both bending and membrane effects are considered). Then, results for different geometric models are presented.

3.2.1 Benchmark problem: Scordelis-Lo Roof

Scordelis-Lo Roof, a benchmark problem for shell elements [50], is cylindrical geometry (length=50m, radius=25) under uniform vertical load $90N/m^2$ (gravity). The material properties are defined as, E=432 MPa and $\nu = 0$. Fig. 16 shows the mesh model in both parametric and physical space; we use CT method for splitting cubic macro-elements and there are 1667 free nodes in domain. The reference solution is the vertical displacement of midside, which is 0.3086 [50]. By using the proposed method, we obtain 0.308 for the midside vertical displacement shown in Fig. 17, which indicates the accuracy and reliability of the current technique.

3.2.2 Complex Geometries

We show that the current technique can be conveniently used to analyze shell structure of complex geometries. First, we apply our method on a shell with single hole. The geometric model is provided in Fig. 18. The structure is under vertical load and the outside boundaries are fixed in all directions. We use quadratic elements for this simulation and macro triangles are split by the PS method (Fig. 19). Also, there are 864 free nodes in the domain. Fig. 20 demonstrates the results of deformation distribution in vertical direction for a shell with single hole.

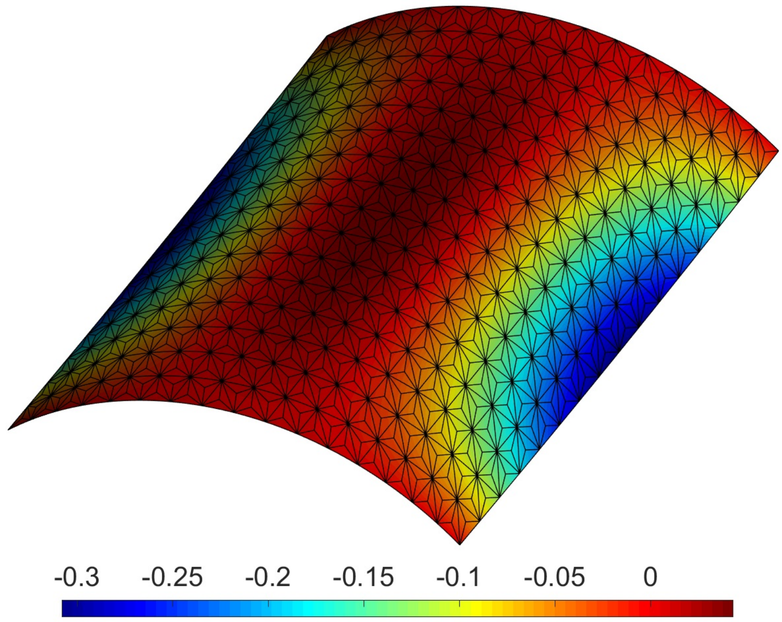

Figure 17: The computed deformation distribution for Scordelis-Lo Roof. The maximum vertical displacement (0.308) occurs in the midside.

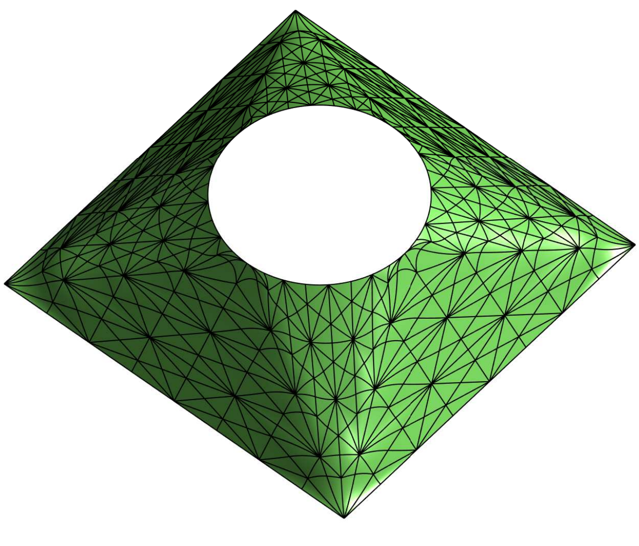

Figure 18: The triangulated geometric model of a shell structure with single hole. This also shows the C1 continuous mesh model with PS split.

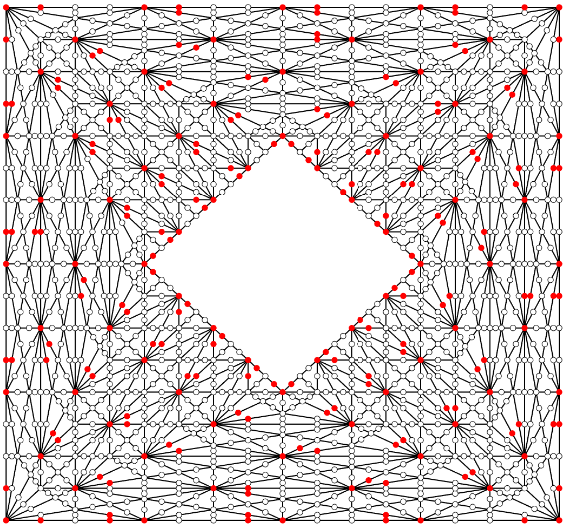

(a) Parametric Domain

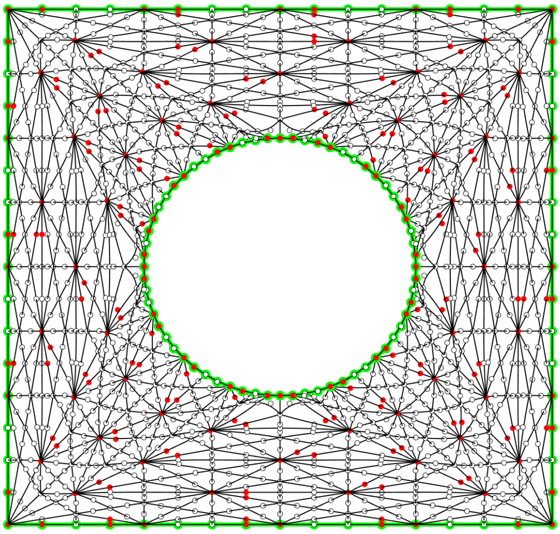

(b) Physical Space

Figure 19: Parametric and physical mesh. We use quadratic triangular elements with PS split.

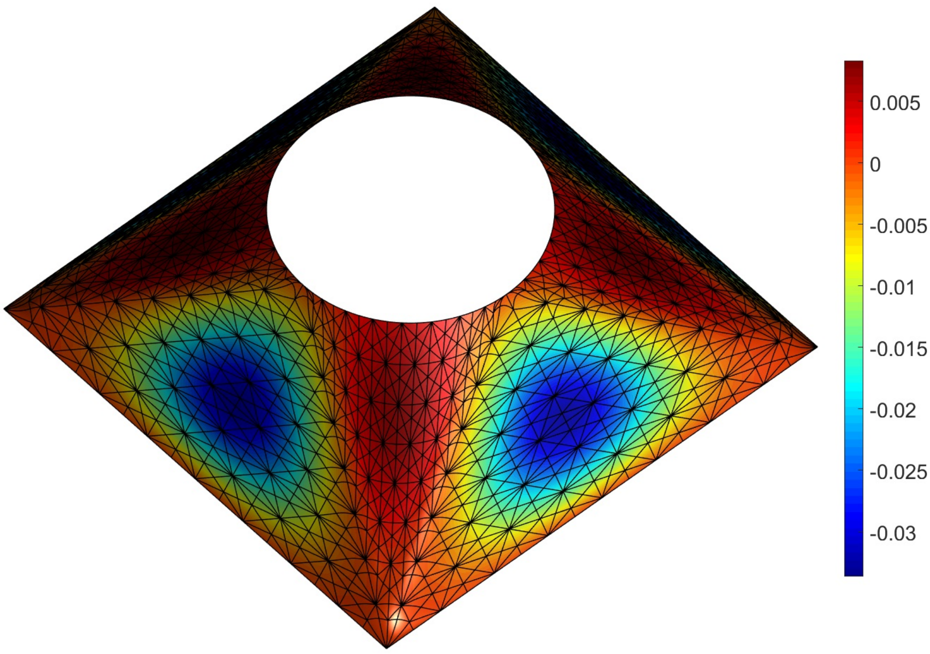

Figure 20: The computed deformation distribution for a shell structure with single hole.

3.2.3 Engineering Practice

In the last example, a car hood is modeled and analyzed. The geometric model of the car hood is extracted from a car cad model available in Grabcad website [designed by F. Kaya and M. Jadhav]. By creating multiple bi-cubic tensor product Bézier patches [twenty patches] over the surface in SolidWorks, the original model is converted to a surface represented by Bézier patches. We use Rhino to convert these cubic patches to quadratic patches since quadratic Bézier patches can be converted to relatively lower order Bézier triangles (Bézier triangles of degree four); therefore, in this work we use quartic Bézier triangles with PS splitting method, generating 3790 free nodes. The Bézier patches are converted to rational Bézier triangles by using in-house codes (Fig. 21). This example demonstrates the applicability of the proposed technique for real engineering problems; this is a significant contribution of our work as geometric models of complex topology are pretty common in engineering practice; moreover, local mesh refinement is typically needed for efficient and accurate simulation. Quartic elements and PS splitting method are used for generating the mesh model in Fig. 22. All the boundaries are fixed in all directions and vertical uniform load is applied on the model. Fig. 23 illustrates the deformation distribution in vertical direction.

Conclusion and Future Works

We developed a rational triangular Bézier spline based isogeometric analysis approach to plate and shell problems. The C1 smoothness of the rTBS elements has allowed us to employ the Kirchhoff-Love formulations. Besides providing the essential continuity over mesh, this technique offers some significant advantages, including those inherited from the concept of isogeometric analysis, for instance preservation of exact geometry representation. Using the rTBS-based isogeometric analysis on several examples, we showed that the presented method enables us to achieve three significant goals: obtaining the optimal or the best possible convergence rate, locally and efficiently refining mesh, and representing a thin geometric model of complex topology. Furthermore, we analyzed a car hood by using the current technique, which demonstrated the functionality of this technique for simulation of real engineering problems. Future work will be focused on development of non-linear shell elements based on rTBS formulation. This will open new opportunities in investigating more engineering problems for which consideration of non-linearity and high accuracy are of particular interest.

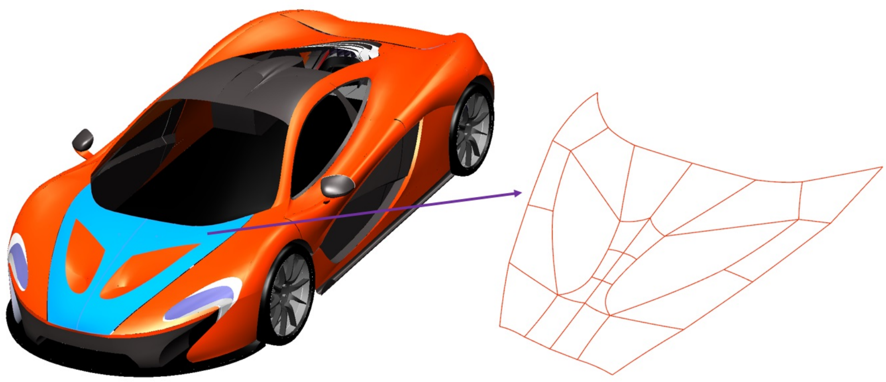

(a) Cad model of a car (extracted from Grabcad website, designed by F. Kaya and M. Jadhav) and its hood represented by multiple Bézier patches

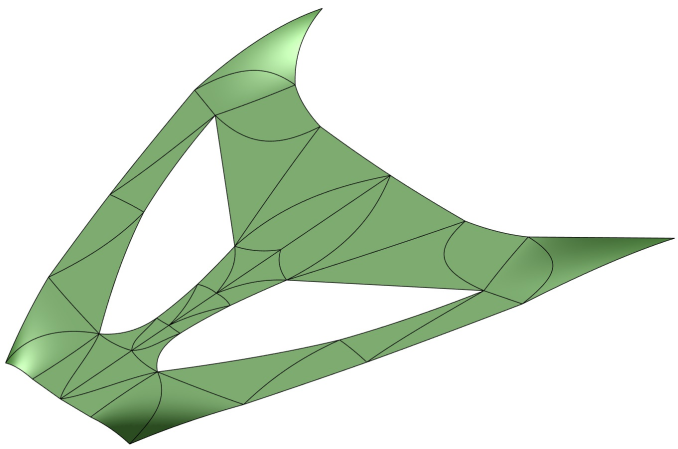

(b) The geometric model of car hood. This model has been created by converting the tensor-product Bézier patches to triangular Bézier patches.

Figure 21: Geometric model of a car hood

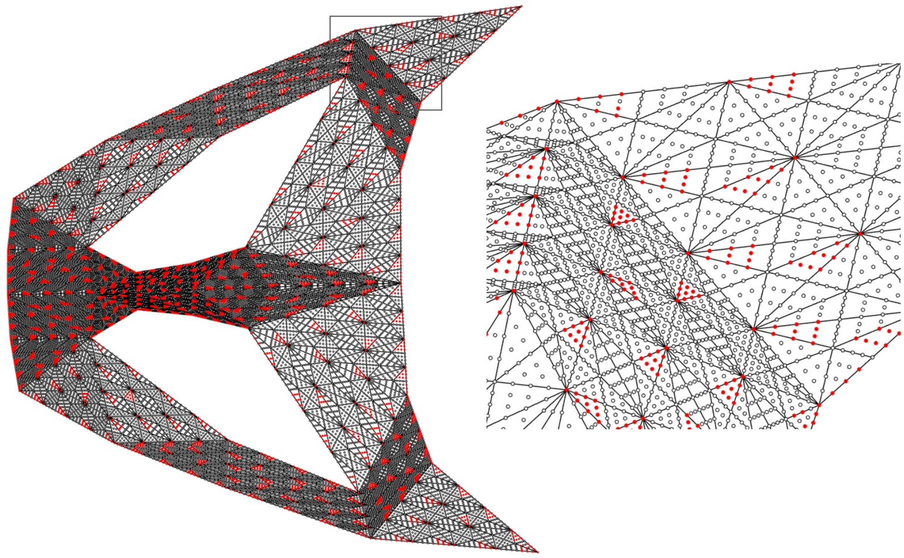

(a) Parametric Domain

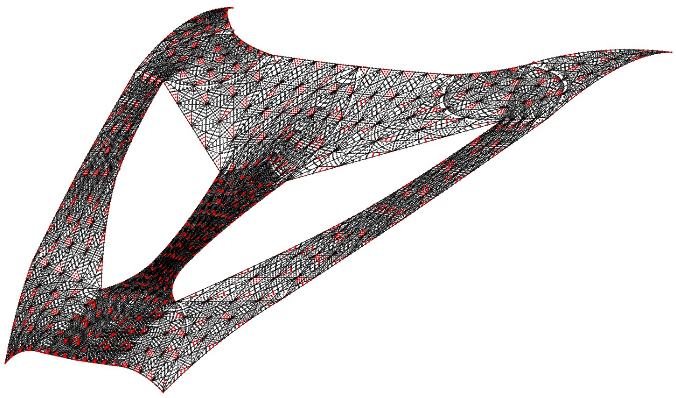

(b) Physical Space

Figure 22: Parametric and physical mesh. We use quartic triangular elements.

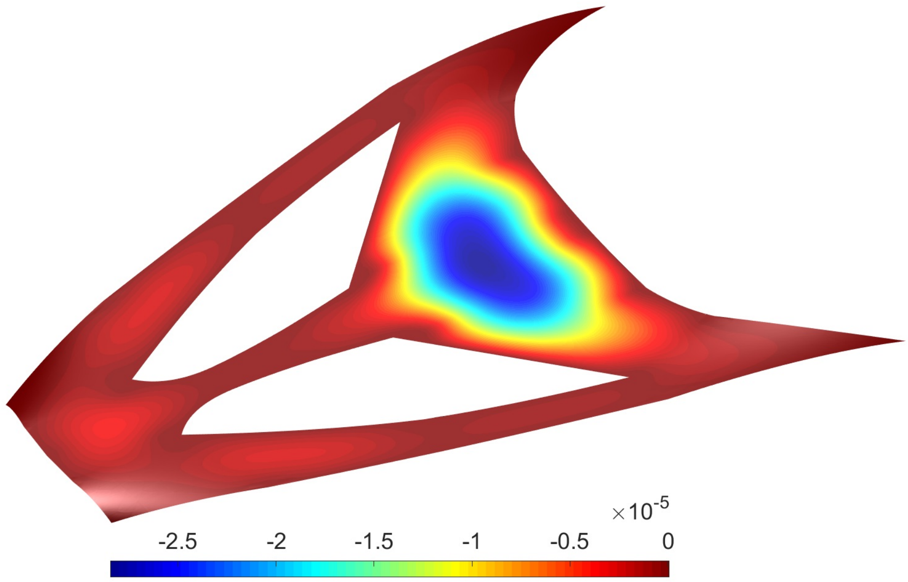

Figure 23: The computed deformation distribution for car hood. The maximum vertical displacement is $28\mu m$.

Acknowledgment

The authors would like to acknowledge the financial support from ARO grant W911NF-17-1-0020 and NSF grant #1435072.

References

[1] M. Radwanska, A. Stankiewicz, A. Wosatko, J. Pamin, Plate and Shell Structures, 2017. doi:10.1002/9781118934531.

[2] M. Bischoff, W. Wall, E. Ramm, Chapter 3 Models and Finite Elements for Thin-walled Structures (1921).

[3] L. Coox, F. Maurin, F. Greco, E. Deckers, D. Vandepitte, W. Desmet, A flexible approach for coupling NURBS patches in rotationless isogeometric analysis of Kirchhoff-Love shells, Computer Methods in Applied Mechanics and Engineering 325 (2017) 505–531. doi:10.1016/j.cma.2017.07.022.

[4] M. Brunet, F. Sabourin, Analysis of a rotation-free 4-node shell element, International Journal for Numerical Methods in Engineering 66 (9) (2006) 1483–1510. doi:10.1002/nme.1608.

[5] H. Stolarski, A. Gilmanov, F. Sotiropoulos, Nonlinear rotation-free three-node shell finite element formulation, International Journal for Numerical Methods in Engineering 95 (9) (2013) 740–770. doi:10.1002/nme.4517.

[6] G. Munglani, R. Vetter, F. K. Wittel, H. J. Herrmann, Orthotropic rotation-free thin shell elements, Computational Mechanics 56 (5) (2015) 785–793. doi:10.1007/s00466-015-1202-x.

[7] E. Oñate, F. Zárate, Rotation-free triangular plate and shell elements, International Journal for Numerical Methods in Engineering 47 (1-3) (2000) 557–603.

[8] H. T. Y. Yang, S. Saigal, A. Masud, R. K. Kapania, A survey of recent shell finite elements, International Journal for Numerical Methods in Engineering 47 (1-3) (2000) 101–127.

[9] M. Bischoff, E. Ramm, Shear deformable shell elements for large strains and rotations, International Journal for Numerical Methods in Engineering (23) 4427–4449. doi:10.1002/(SICI)1097-0207(19971215)40:23¡4427::AID-NME268¿3.0.CO;2-9.

[10] T. X. Duong, F. Roohbakhshan, R. A. Sauer, A new rotation-free isogeometric thin shell formulation and a corresponding continuity constraint for patch boundaries, Computer Methods in Applied Mechanics and Engineering 316 (2017) 43–83. doi:10.1016/j.cma.2016.04.008.

[11] S. Green, G. M. Turkiyyah, A rotation-free quadrilateral thin shell subdivision finite element, Communications in Numerical Methods in Engineering 21 (12) (2005) 757–767. doi:10.1002/cnm.791.

[12] F. Cirak, Q. Long, Advances in subdivision finite elements for thin shells, New Trends in Thin Structures: Formulation, Optimization and Coupled Problems (2010) 205–227.

[13] F. Zárate, E. Oñate, Extended rotation-free shell triangles with transverse shear deformation effects, Computational Mechanics 49 (4) (2012) 487–503. doi:10.1007/s00466-011-0653-y.

[14] L. Noels, R. Radovitzky, A new discontinuous Galerkin method for Kirchhoff-Love shells, Computer Methods in Applied Mechanics and Engineering 197 (33-40) (2008) 2901–2929. doi:10.1016/j.cma.2008.01.018.

[15] G. Becker, C. Geuzaine, L. Noels, A one field full discontinuous Galerkin method for Kirchhoff-Love shells applied to fracture mechanics, Computer

Methods in Applied Mechanics and Engineering 200 (45-46) (2011) 3223–3241. doi:10.1016/j.cma.2011.07.008.

[16] L. Greco, M. Cuomo, L. Contrafatto, A quadrilateral G1-conforming finite element for the Kirchhoff plate model, Computer Methods in Applied Mechanics and Engineering (2018) 1–39doi:10.1016/j.cma.2018.09.028.
URL https://doi.org/10.1016/j.cma.2018.09.028

[17] J. Altenbach, H. Altenbach, V. A. Eremeyev, On generalized Cosserat-type theories of plates and shells: a short review and bibliography, Archive of Applied Mechanics 80 (1) (2010) 73–92. doi:10.1007/s00419-009-0365-3.

[18] H. Altenbach, V. A. Eremeyev, L. P. Lebedev, Micropolar Shells as Two-dimensional Generalized Continua Models, Springer Berlin Heidelberg, Berlin, Heidelberg, 2011, pp. 23–55. doi:10.1007/978-3-642-19219-7-2.

[19] L. Greco, M. Cuomo, L. Contrafatto, A reconstructed local B formulation for isogeometric Kirchhoff-Love shells, Computer Methods in Applied Mechanics and Engineering 332 (2018) 462–487. doi:10.1016/j.cma.2018.01.005.

[20] T. J. R. Hughes, J. A. Cottrell, Y. Bazilevs, Isogeometric analysis: CAD, finite elements, NURBS, exact geometry and mesh refinement, Computer Methods in Applied Mechanics and Engineering 194 (39) (2005) 4135–4195. doi:https://doi.org/10.1016/j.cma.2004.10.008.

[21] X. Du, G. Zhao, W. Wang, Nitsche method for isogeometric analysis of Reissner-Mindlin plate with non-conforming multi-patches, Computer Aided Geometric Design 35-36 (2015) 121–136. doi:10.1016/j.cagd.2015.03.005.

[22] J. Kiendl, K. U. Bletzinger, J. Linhard, R. Wüchner, Isogeometric shell analysis with Kirchhoff-Love elements, Computer Methods in Applied Mechanics and Engineering 198 (49-52) (2009) 3902–3914. doi:10.1016/j.cma.2009.08.013.

[23] D. J. Benson, Y. Bazilevs, M. C. Hsu, T. J. R. Hughes, Isogeometric shell analysis: The Reissner-Mindlin shell, Computer Methods in Applied Mechanics and Engineering 199 (5-8) (2010) 276–289. doi:10.1016/j.cma.2009.05.011.

[24] C. H. Thai, H. Nguyen-Xuan, N. Nguyen-Thanh, T.-H. Le, T. Nguyen-Thoi, T. Rabczuk, Static, free vibration, and buckling analysis of laminated composite Reissner-Mindlin plates using NURBS-based isogeometric approach, International Journal for Numerical Methods in Engineering 91 (6) (2012) 571–603. doi:10.1002/nme.4282.

[25] W. Dornisch, S. Klinkel, B. Simeon, Isogeometric Reissner-Mindlin shell analysis with exactly calculated director vectors, Computer Methods in Applied Mechanics and Engineering 253 (2013) 491–504. doi:10.1016/j.cma.2012.09.010.

[26] W. Dornisch, S. Klinkel, Treatment of Reissner-Mindlin shells with kinks without the need for drilling rotation stabilization in an isogeometric framework, Computer Methods in Applied Mechanics and Engineering 276 (2014) 35–66. doi:10.1016/j.cma.2014.03.017.

[27] P. Kang, S.-K. Youn, Isogeometric analysis of topologically complex shell structures, Finite Elements in Analysis and Design 99 (2015) 68–81. doi:10.1016/j.finel.2015.02.002.

[28] Z. Lei, F. Gillot, L. Jezequel, Developments of the mixed grid isogeometric Reissner-Mindlin shell: Serendipity basis and modified reduced quadrature, European Journal of Mechanics, A/Solids 54 (2015) 105–119. doi:10.1016/j.euromechsol.2015.06.010.

[29] R. Echter, B. Oesterle, M. Bischoff, A hierarchic family of isogeometric shell finite elements, Computer Methods in Applied Mechanics and Engineering 254 (2013) 170–180. doi:10.1016/j.cma.2012.10.018.

[30] R. Bouclier, T. Elguedj, A. Combescure, An isogeometric locking-free NURBS-based solid-shell element for geometrically nonlinear analysis (December 2014) (2015) 774–808. doi:10.1002/nme.

[31] S. Hosseini, J. J. C. Remmers, C. V. Verhoosel, R. de Borst, An isogeometric continuum shell element for non-linear analysis, Computer Methods in Applied Mechanics and Engineering 271 (2014) 1–22. doi:10.1016/j.cma.2013.11.023.

[32] S. Hosseini, J. J. C. Remmers, C. V. Verhoosel, R. De Borst, An isogeometric solid-like shell element for nonlinear analysis, International Journal for Numerical Methods in Engineering 95 (3) (2013) 238–256. doi:10.1002/nme.4505.

[33] D. J. Benson, S. Hartmann, Y. Bazilevs, M.-C. Hsu, T. J. R. Hughes, Blended isogeometric shells, Computer Methods in Applied Mechanics and Engineering 255 (2013) 133–146. doi:10.1016/j.cma.2012.11.020.

[34] S. Xia, X. Wang, X. Qian, Continuity and convergence in rational triangular Bézier spline based isogeometric analysis, Computer Methods in Applied Mechanics and Engineering 297 (2015) 292–324. doi:https://doi.org/10.1016/j.cma.2015.09.001.

[35] C. Wang, S. Xia, X. Wang, X. Qian, Isogeometric shape optimization on triangulations, Computer Methods in Applied Mechanics and Engineering 331 (2018) 585–622. doi:https://doi.org/10.1016/j.cma.2017.11.032.

[36] Y. Bazilevs, V. M. Calo, J. A. Cottrell, J. A. Evans, T. J. R. Hughes, S. Lipton, M. A. Scott, T. W. Sederberg, Isogeometric analysis using T-splines, Computer Methods in Applied Mechanics and Engineering 199 (5) (2010) 229–263. doi:https://doi.org/10.1016/j.cma.2009.02.036.

[37] L. Engvall, J. A. Evans, Isogeometric unstructured tetrahedral and mixed-element BernsteinBézier discretizations, Computer Methods in Applied Mechanics and Engineering 319 (2017) 83–123. doi:10.1016/j.cma.2017.02.017.

[38] N. Nguyen-Thanh, J. Kiendl, H. Nguyen-Xuan, R. Wüchner, K. U. Bletzinger, Y. Bazilevs, T. Rabczuk, Rotation free isogeometric thin shell analysis using PHT-splines, Computer Methods in Applied Mechanics and Engineering 200 (47-48) (2011) 3410–3424. doi:10.1016/j.cma.2011.08.014.

[39] Y. Guo, J. Heller, T. J. Hughes, M. Ruess, D. Schillinger, Variationally consistent isogeometric analysis of trimmed thin shells at finite deformations, based on the STEP exchange format, Computer Methods in Applied Mechanics and Engineering 336 (2018) 39–79. doi:10.1016/j.cma.2018.02.027.

[40] J. Kiendl, Y. Bazilevs, M. C. Hsu, R. Wüchner, K. U. Bletzinger, The bending strip method for isogeometric analysis of Kirchhoff-Love shell structures comprised of multiple patches, Computer Methods in Applied Mechanics and Engineering 199 (37-40) (2010) 2403–2416. doi:10.1016/j.cma.2010.03.029.
URL `http://dx.doi.org/10.1016/j.cma.2010.03.029`

[41] N. Jaxon, X. Qian, Isogeometric analysis on triangulations, Computer-Aided Design 46 (2014) 45 – 57. doi:https://doi.org/10.1016/j.cad.2013.08.017.

[42] S. Xia, X. Qian, Isogeometric analysis with bézier tetrahedra, Computer Methods in Applied Mechanics and Engineering 316 (2017) 782 – 816. doi:https://doi.org/10.1016/j.cma.2016.09.045.

[43] N. Liu, A. E. Jeffers, A geometrically exact isogeometric Kirchhoff plate: feature-preserving automatic meshing and C^1 rational triangular Bézier spline discretizations, International Journal for Numerical Methods in Engineering (August 2017) (2018) 1–15. doi:10.1002/nme.5809.

[44] F. Maurin, F. Greco, L. Coox, D. Vandepitte, W. Desmet, Isogeometric collocation for Kirchhoff-Love plates and shells, Computer Methods in Applied Mechanics and Engineering 329 (2018) 396–420. doi:10.1016/j.cma.2017.10.007.

[45] M.-J. Lai, L. L. Schumaker, Spline Functions on Triangulations, Encyclopedia of Mathematics and its Applications, Cambridge University Press, 2007. doi:10.1017/CBO9780511721588.

[46] J. N. Lyness, R. Cools, A survey of numerical cubature over triangles, Proceedings of Symposia in Applied Mathematics American Mathematical Society Providence, RI 48. doi:10.1090/psapm/048/1314845.

[47] S. Timoshenko, S. Woinowsky-Krieger, Theory of Plates and Shells (1959).

[48] A. Tagliabue, L. Dedè, A. Quarteroni, Isogeometric Analysis and error estimates for high order partial differential equations in fluid dynamics, Computers and Fluids 102 (2014) 277–303. doi:10.1016/j.compfluid.2014.07.002.
URL `http://dx.doi.org/10.1016/j.compfluid.2014.07.002`

[49] A. Bartezzaghi, L. Dedè, A. Quarteroni, Isogeometric Analysis of high order Partial Differential Equations on surfaces, Computer Methods in Applied Mechanics and Engineering 295 (2015) 446–469. doi:10.1016/j.cma.2015.07.018.

[50] R. H. Macneal, R. L. Harder, A proposed standard set of problems to test finite element accuracy, Finite Elements in Analysis and Design 1 (1) (1985) 3 – 20. doi:https://doi.org/10.1016/0168-874X(85)90003-4.